Pergamon

Journal of Structural Geology, Vol. 18, No. 1, pp. 109 to 119, 1996

0191-8141/96 $15.00 + 0.00

0191-8141(95)00086-0

Numerical modelling of the effects of fault slip on fluid flow around extensional faults

XING ZHANG and DAVID J. SANDERSON

Geomechanics Research Group, Department of Geology, University of Southampton, Southampton SO17 1BJ, U.K.

(*Received* 3 *August* 1994; *accepted in revised form* 11 *July* 1995)

Abstract—Fluid flow and deformation in regions of fractured rock around extensional faults have been modelled using distinct element methods (UDEC code). The basic methodology is described in terms of a simple model of a planar normal fault zone, at the Earth's surface. The model is then modified to simulate deformation at greater depths and to investigate irregularities in fault shape (including dilational and anti-dilational fault jogs). The results obtained show that the deformation of a faulted region resulted in significant variation in fracture dilation (porosity), stress distribution, fluid pressure and fluid flow.

The geometry of models and the applied boundary conditions had important effects on deformation and fluid flow. At shallow depth, dilation and fluid flow occurred both in the fault zone and the hangingwall, with little change in the footwall. At greater depth, the higher compressive stresses tended to close all fractures, except within the fault zone where the shear displacements caused local dilation. The presence of anti-dilational bends reduced the dilation and fluid flow in the fault zone, but promoted greater deformation in parts of the hangingwall. The dynamic response of fracture aperture, pore pressure and shear displacement to fault slip was also studied. The modelled results are in reasonable correspondence with observed natural examples and have practical significance for evaluating fluid flow and deformation in regions which exhibit normal faulting.

INTRODUCTION

Faults are found nearly everywhere in the upper crust and may act as major channel-ways for concentrated fluid flow. A range of phenomena from earthquakes to hydrocarbon migration and hydrothermal ore deposits are directly related to faulting, fluid flow and their interaction. In addition, there is abundant evidence that the passage of fluids in faulted areas is episodic and linked to increments of fault slip (Sibson 1990). Such evidence includes reservoir-induced seismicity, earthquakes triggered by fluid injection, forced oil recovery and waste disposal (Healy *et al.* 1968, Raleigh *et al.* 1976, Das & Scholz 1981, Talwani & Acree 1985, Knipe 1993). Hence, it is fundamentally important to have a quantitative understanding of fracture dilation, fault slip and fluid pressure variation during periods of deformation. Moreover, it is desirable to evaluate the permeability and porosity (opening between blocks) within a faulted region both during and after movement.

In this work, movement on an extensional fault is simulated by distinct element methods using a version of the Universal Distinct Element Code (UDEC), developed by P.A. Cundall and marketed by ITASCA Consulting Group Inc., of Minneapolis, Minnesota, U.S.A. The source code was available, thus allowing modifications to be made.

The models were developed to simulate a normal fault affecting a fractured (jointed) layer above a basement block. Displacement of the basement block induces deformation with resultant dilation and slip within the fractured rock mass. Fluid pressure and fluid flow in the region were investigated quantitatively. The modelling technique is described for an initial model involving a relatively simple planar fault zone at shallow depths (0–40 m), where the fluid pressure is assumed to be hydrostatic. The behaviour at greater depths (2 km), with supra-hydrostatic fluid pressures, is then discussed. The geometry of the fault zone was modified to incorporate dilational and anti-dilational jogs. Finally, the dynamic response of fluid dilation interactions is discussed.

OUTLINE OF MODELLING

Basic geometry—model A

The initial geological model comprises two types of structures (Fig. 1).

(1) A major extensional fault is represented as a 2.5 m wide zone, dipping at 65°, and is modelled as a highly fractured zone with two sets of fractures (parallel and orthogonal to the fault zone) defining blocks of 0.833 × 0.833 m.

(2) Regional scale fractures (joints) are represented as two sets of fractures having the following features:

(a) A sub-vertical set (±2°) of extensional fractures, consistent with σ_3 being sub-horizontal in extensional regions. Some fractures of this set were allowed to extend to the lower boundary. The lengths of the fractures were sampled from a power-law distribution with an exponent (D) = 1.6, with a lower limit of the fracture length of 5 m. Heffer & Brown (1990) stated that the power-law exponent (fractal dimension) of fracture size approaches 3 in a two-dimensional case, but other

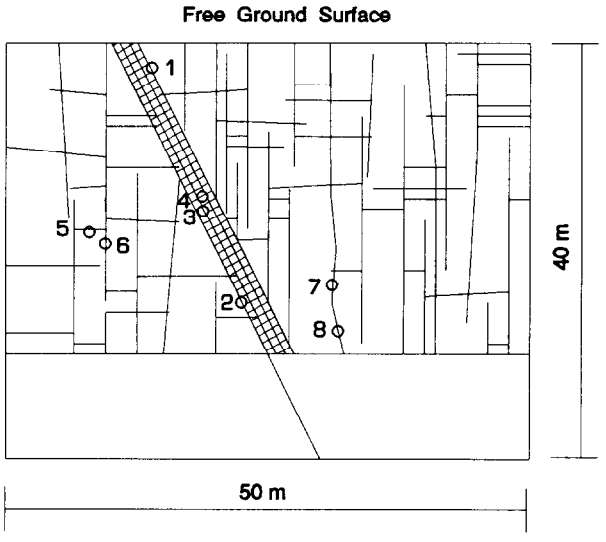

Fig. 1. Geometry of model A which consists of a faulted region with a straight fault zone and regional joints above an unjointed basement; numbers refer to monitoring system, see text.

investigators have noted fractal dimensions between 0.9 and 1.7 (Segall & Pollard 1983, Barton & Hsieh 1989, Sanderson & Zhang unpubl. observations).

(b) A flat-lying set of shorter cross-fractures are horizontal (±5°) and generally abut the sub-vertical set. In the models the probability of a cross-fracture stopping at a pre-existing sub-vertical fracture was set at 0.9, a value consistent with some natural examples given by Lorenz *et al.* (1991) and Lorenz & Finley (1991). As a result, the length distribution of the flat-lying fractures is mainly dependent on the spacing of the sub-vertical fractures.

For both sets of fractures, their mid-points were randomly located with a uniform distribution in both the x and y directions. The sub-vertical fractures were assigned a larger hydraulic aperture, twice that of the cross-fractures, because the sub-vertical fractures are longer and normal to the minimum principal stress σ_3.

The size of the simulated region was 40 m in height and 50 m in width (Fig. 1). It is relatively easy to change the scale of the model and adjust the boundary conditions on the free surface to simulate greater depths, as discussed later.

UDEC implementation

In UDEC modelling, the deformation of the fractured rock consists of the elastic deformation of blocks of intact rock and of displacements along and across fractures (Cundall *et al.* 1978). The amount of normal and tangential displacement between two adjacent blocks can be determined directly from block geometry, and block centroid translation and rotation. The force–displacement law relates incremental normal and shear forces ($\partial \mathbf{F}_n$, $\partial \mathbf{F}_s$) to the amount of relative incremental displacements (∂U_n, ∂U_s):

$$\partial \mathbf{F}_n = \mathbf{K}_n \, \partial U_n \tag{1}$$

$$\partial \mathbf{F}_s = \mathbf{K}_s \, \partial U_s \tag{2}$$

where $\mathbf{K}_n$ and $\mathbf{K}_s$ are the contact normal and shear stiffness respectively. Such force–displacement relationships allow the evaluation of shear and normal forces between the intact blocks in a deformed region of fractured rock. The deformability of the interface between blocks and frictional characteristics are represented by spring-slider systems with prescribed force–displacement relations which allow evaluation of shear and normal forces between blocks.

In UDEC, a fully coupled mechanical–hydraulic analysis is performed, where fracture conductivity is dependent on mechanical deformation and displacement, and conversely, fluid pressure affects the mechanical behaviour (Pine & Cundall 1985, Last & Harper 1990). For a closely packed system of blocks, there exists a network of domains, each of which is assumed to be filled with fluid under pressure and to communicate with its neighbours through contacts.

When a pressure differential, Δp, exists between adjacent domains, flow will take place. The flow rate is calculated in two different ways depending on the type of contact. For a point contact (i.e. corner–edge or corner–corner), the flow-rate, q, is:

$$q = -k_c \, \Delta p \tag{3}$$

where k_c is a contact permeability parameter, related to the geometry of a domain. At edge–edge contacts, calculation is based on the cubic law of flow in fractures (Snow 1968, Louis 1969, Witherspoon *et al.* 1980, Barton *et al.* 1985). The flow rate is then given by:

$$q = -k_j a^3 \, \Delta p / l \tag{4}$$

where k_j is a joint permeability factor; a is the hydraulic aperture, and l is the contact length.

In the absence of gravity, Δp is given by the pressure differential between the domains. Where gravity is taken into account, Δp is given by:

$$\Delta p = p_1 - p_2 - \rho_w g (y_2 - y_1) \tag{5}$$

where p_1, p_2 are the hydraulic pressures of two adjacent domains, y_1, y_2 are the y-coordinates of the domain centres, and ρ_w is fluid density.

The hydraulic aperture, a, is given by:

$$a = a_0 + u_n \tag{6}$$

in which a_0 is the aperture at zero normal effective stress, and u_n is the contact normal displacement.

A minimum value, a_{res}, is assumed for an aperture, beyond which mechanical closure does not affect the contact permeability. Where pore pressure exceeds the normal stress acting on a fracture, it is possible to open the fracture so that the aperture is larger than a_0. Hence, a compressive effective stress can cause apertures to

close and a tensile effective stress can cause apertures to open. Thus, normal displacement is given by:

$$u_n = \sigma_n k_a + a_0 \quad (7)$$

where k_a is a factor related to rock property.

Boundary conditions and material properties

Elastic constitutive behaviour of the material was selected, which means that the deformation was accommodated by elastic strain of the blocks and dilation and slip between blocks. In the models, the rock parameters were selected to represent a tight sandstone (Table 1), based on data taken from a number of sources (Rosso 1976, Jaeger & Cook 1979, Barton *et al.* 1985, Pine & Cundall 1985, Yoshnaka & Yamabe 1986, Last & Harper 1990).

During the deformation, the vertical stress σ_1 was caused by gravitational loading and σ_3 was in a horizontal direction. The ratio between the horizontal stress (σ_3) and overburden stress (σ_1) was 0.45. The base of the hangingwall block was allowed to move with a constant velocity parallel to the fault. No vertical movement of the base of the footwall was allowed, thus generating a relative displacement of the two blocks.

At shallow crustal depths, the head of fluid pressure in the model was selected to be hydrostatic ($\lambda_w = 0.4$), i.e. 10 MPa km^{-1} (Yerkes *et al.* 1985, Sibson 1990). The hydraulic pressure along the top and bottom boundaries was set to 0 and 400 KPa, respectively, with a downward linear increase in hydraulic pressure applied along the left and right boundaries. Note that the magnitude of fluid pressure was a little lower than that of the horizontal compressive stress, so that the effective stress in that direction (σ_3') was still compressive. However, σ_3' had a very small value (0.05 overburden), while the value of effective stress σ_1' in the vertical direction was much higher (0.6 overburden), as shown in Fig. 2.

Table 1. Material properties used for modelling

	Value	Units
Block property		
Density	2500	kg m^{-3}
Shear modulus	13.46	GPa
Bulk modulus	24.3	GPa
Young's modulus	35	GPa
Poisson's ratio	0.26	
Fracture property		
Tensile strength	0	MPa
Cohesion	0	MPa
Friction angle	35	degree
Dilation angle	5	degree
Joint normal stiffness	24.3	GPa m^{-1}
Joint shear stiffness	13.46	GPa m^{-1}
Residual aperture		
(vert. fracture)	0.0002	m
(cross-fracture)	0.0001	m
Zero stress aperture		
(vert. fracture)	0.001	m
(cross-fracture)	0.0005	m
Fluid property		
Density	1000	kg m^{-3}
Viscosity	0.00035	Pa s
Bulk stiffness	3	GPa

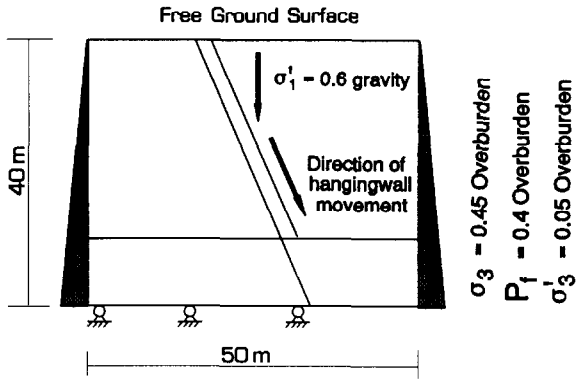

Fig. 2. Mechanical and hydraulic boundary conditions at a shallow depth in model A. The vertical stress σ_1 is due to gravity (overburden) and the laterally compressive stress σ_3 is 0.45 σ_1; fluid pressure is applied along the left and right boundaries and increases linearly downwards; the effective stress in the horizontal direction (σ_3') has a small compressive value of 0.05 overburden.

Monitoring system

The UDEC allows a number of physical parameters, such as stress, displacement, dilation, flow rate and fluid pressure, to be monitored during modelling. In this study, a total of 40 monitors were set at eight points, to monitor pore pressure, dilation of fractures, slip, shear stress and normal stress. There were four locations in the fault zone, together with two in the footwall and two in the hangingwall. The selection of monitored positions was designed to cover different areas (fault zone, footwall and hangingwall), levels (near to the top surface, near to the basement rocks) and fracture types (extensional fracture, cross fracture). The fracture positions monitored are shown in Fig. 1.

In the models, the 'porosity', P_0, is defined as the ratio:

$$P_0 = O_a/R_a \quad (8)$$

in which O_a is the sum of all openings and R_a is the area of the studied region. Clearly such a parameter, P_0, is directly related to the dilation of fractured rocks, and is indirectly related to the pore pressure and permeability of fractured rocks.

Modelling was carried out on an IBM RS-6000 workstation; typical modelling runs lasted 6 h.

STRESS DISTRIBUTION AND FLUID FLOW IN MODEL A AT A SHALLOW DEPTH WITH A HYDROSTATIC FLUID PRESSURE

The results from model A (Fig. 1) will be described in some detail in this section, since they both demonstrate the general approach to modelling using UDEC and show much of the intrinsic value of such models in the interpretation of fluid flow as a result of extensional faulting in general. The other models will be described in relation to this basic model, with discussion limited to significant variations in procedure or result.

Stress redistribution and dilation

Once the basic geometry and properties of the model have been specified, an initial stage in the modelling involves the achievement of steady-state mechanical and hydraulic conditions. The basement beneath the area was fixed so that no movement occurred in the vertical direction. All blocks were gravitationally loaded until an approximate mechanical balance was achieved. Hydrostatic pressure was then applied along the boundaries. Figure 3 shows the stress distribution around the free surface and the basement of the modelled region. The stress within the region is approximately uniform, being dominated by the gravitational loading, but block geometry produces some significant modifications, particularly near to the fault zone.

Faulting was simulated by allowing movement of the basement beneath the hangingwall region to a total throw of 0.4 m. This subsidence was achieved in 1 s and was monitored for a further second, during which the recovery of stress, dilation and fluid pressure in the fault region began.

The amounts of dilation, slip, fluctuation in fluid pressure and associated permeability change as a result of the subsidence and extension of the hangingwall. Figure 4 shows the geometry and stress redistribution of the same local areas as in Fig. 3.

The maximum stress was 0.277 MPa near the surface and 1.11 MPa at the base prior to faulting (Fig. 3), and 0.568 MPa around the surface and 14.28 MPa around the base after faulting (Fig. 4).

The distribution of aperture throughout the model prior to fault slip is shown in Fig. 5(a). During fault movement, relative displacement occurs between blocks, producing changes in the aperture of fractures (Fig. 5b). It is interesting to note that dilation occurred mainly within the fault zone and the hangingwall, with little in the footwall. One of the reasons for this is that the shear resistance of the sub-horizontal fractures within the fault zone and hangingwall is reduced, allowing greater opening and displacement, which in turn allowed opening of the sub-vertical fractures (Fig. 5); note that Fig 5(a) represents aperture values ≥ 0.0012 m, whereas Fig. 5(b) shows apertures ≥ 0.004 m. In addition to dilation, slip on fractures in the fault zone and hangingwall produced some block rotation and accompanying dilation (Fig. 4).

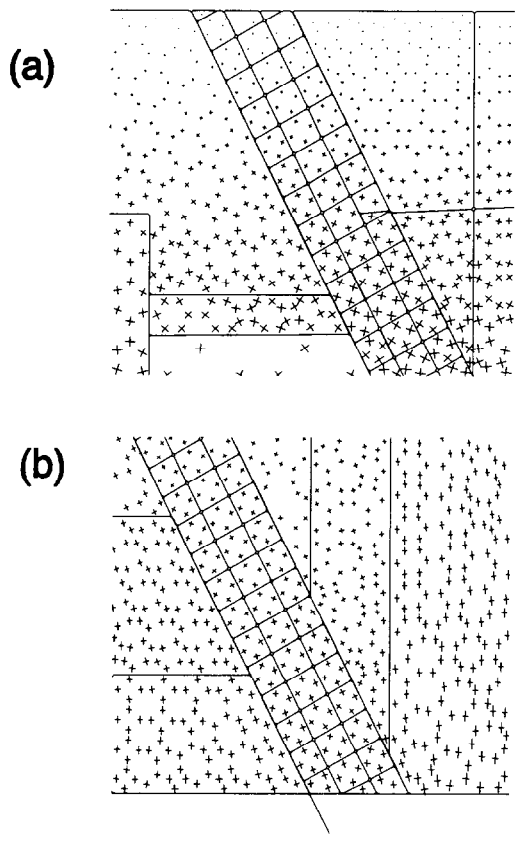

Fig. 3. Principal stress distribution of local regions of model A before fault movement. The directions and magnitudes of two principal stresses at an element are indicated with a cross. The basement beneath this area was fixed so that no movement occurred in the vertical direction. All blocks were subjected to the gravitational loading until an approximate mechanical balance was achieved, then hydrostatic pressure was applied. The resulting stress state has been modified by the fracture geometry and fluid flow. (a) Principal stress distribution at the surface; the maximum value of major principal stress is 0.277 MPa. (b) Principal stress distribution at the base; the maximum value of principal stress is 1.1 MPa.

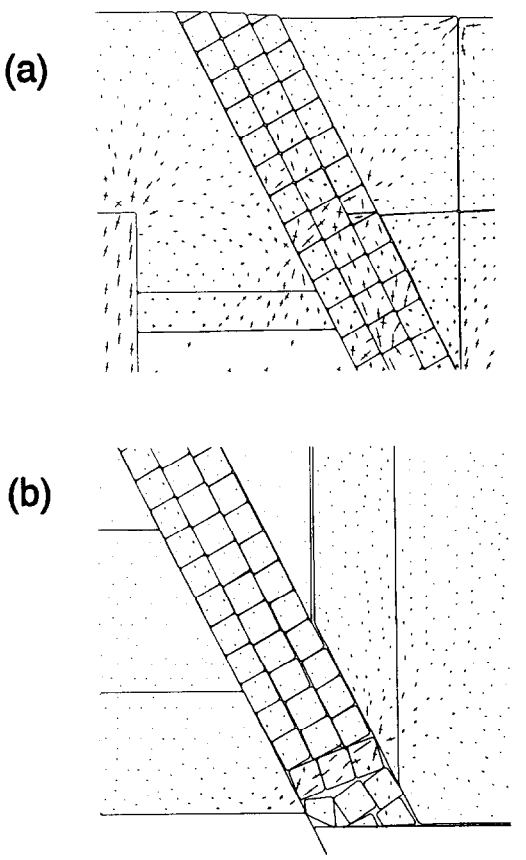

Fig. 4. Internal structures and stress redistribution in local regions of model A after fault slip, which produced significant movement and rotation of the blocks. Compared with the stress distribution in Fig. 3, there is an increase due to compressive contacts around some blocks and a reduction due to openings around others. (a) Stress state at the surface; the maximum value of stress is 0.568 MPa. (b) Stress state at the base; the maximum value of stress is 14.28 MPa.

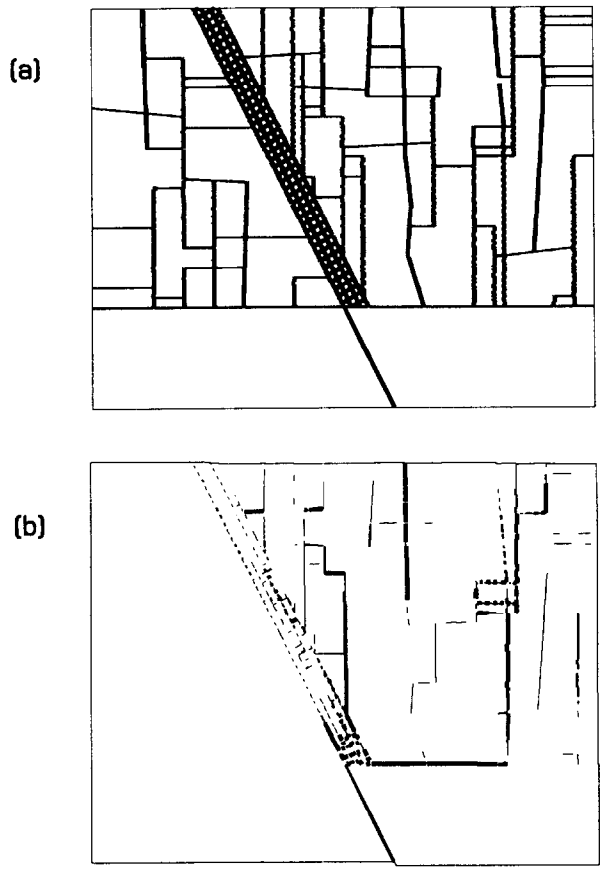

Fig. 5.(a) The apertures before fault slip show a uniform distribution; each line represents an aperture value of 0.0012 m and only those apertures which exceeded this value are shown. (b) After fault slip, apertures increase in the fault zone and hangingwall; each line indicates an aperture value of 0.004 m and only those apertures which exceeded this value are shown.

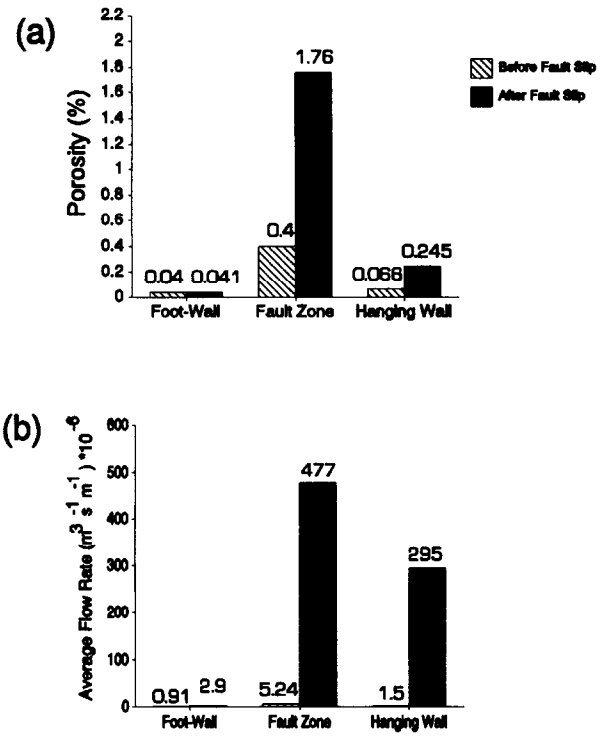

Fig. 6.(a) Quantitative comparisons of percentage porosity in different areas (footwall, fault zone and hangingwall). After fault slip, the porosity of the fault zone and hangingwall increased to 1.76 and 0.25%, respectively (approximately 4× higher than before faulting); the porosity of the footwall changed little. (b) Quantitative comparison of flow rates before and after fault slip. The average flow rate in the fault zone and hangingwall increased by two orders of magnitude after fault slip.

Porosity and permeability changes

Quantitative comparisons of the porosity of the footwall, fault zone and hangingwall regions of the model are shown in Fig. 6(a). The initial extensional fractures were set at the same aperture, so the initial porosity was determined by the density and connectivity of the fractures. Before faulting, the fault zone had a relatively high porosity of 0.4% and the country rocks had relatively low values of 0.04 and 0.066% for the footwall and the hangingwall, respectively. After faulting, the 'porosity' of the fault zone and the hangingwall increased greatly to 1.76 and 0.25%; 4.4× and 3.73× higher than values before faulting. The 'porosity' of the footwall was little changed.

Many geological phenomena may be related to such changes in the capacity of the fractures to store fluids, ranging from the fracture porosity of hydrocarbon reservoirs to potential sites for precipitation from ore-bearing fluids. It should be noted that dilation occurred on both vertical and horizontal fractures, and in many cases shear produced localized dilational jogs. These phenomena and their significance in fault tectonics and mineralization have been discussed by Sibson (1989a) amongst others.

After faulting, the apertures of fractures within the fault zone and the hangingwall increased greatly and, at the −15 m level, were approximately one order of magnitude higher than those within the footwall. Corresponding to this increase in aperture, the fluid pressure at this level had a slight decrease (from 0.152 to 0.149 MPa), probably due to the opening of extensional fractures at rates faster than fluids could flow in to restore equilibrium. Such fluid pressure reduction in local areas is consistent with the suction-pump mechanism of Sibson (1989a, 1990).

The flow rate within the fault zone and the hangingwall had an abrupt increase due to the increase in aperture. Figure 7(a) shows the pathways and directions of fluid flow before faulting; there was a fairly uniform flow rate through fractures in the whole region. However, after faulting, the fluids mainly flowed through the fault zones and hangingwall, as shown in Fig. 7(b); note that the minimum value of flow rate shown in Fig. 7(a) is 10×10^{-6} m^3 s^{-1} m^{-1}, whereas it is 50×10^{-6} m^3 s^{-1} m^{-1} in Fig. 7(b). A summary of average flow rates (volume rates of flow per area) before and after faulting is shown in Fig. 6(b). This average flow rate is the mean value of three measurements of flow rate through the top boundary, the bottom boundary and the middle section. The average flow rate in the footwall was three times higher than before fault slip. However, the flow rate in the fault zone and hangingwall was two orders of magnitude higher after faulting than before. The flow rate between parallel plates is dependent on the cube of

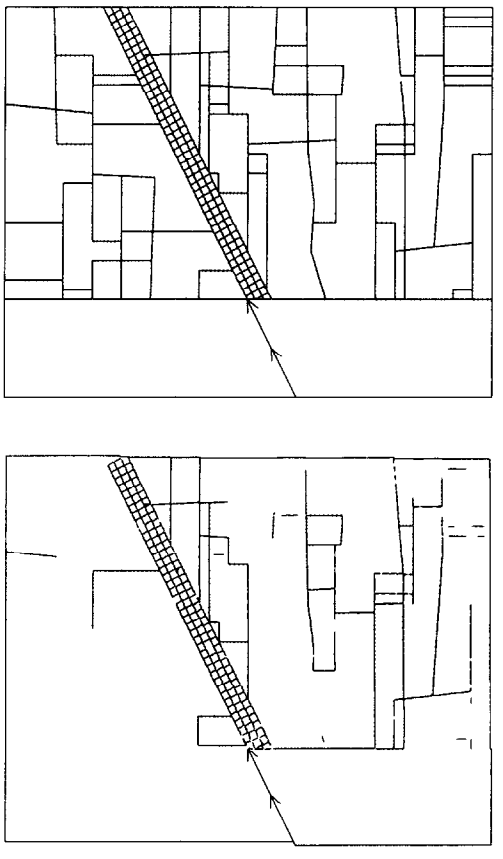

Fig. 7. Pathways and directions of fluid flow. (a) Before fault slip, fluids flowed upwards at a fairly uniform flow rate throughout the whole region; the minimum value of flow rate in an individual fracture was 10×10^{-6} m^3 s^{-1} m^{-1}. (b) After fault slip, fluids mainly flowed through the fault zone and hangingwall; the minimum value of flow rate in an individual fracture was 50×10^{-6} m^3 s^{-1} m^{-1}.

the aperture, hence a large permeability increase is expected for any significant increase in dilation. It is important to note that the dilational structures created in the vertical section are also likely to form channels normal to the plane of section, which, in the presence of out-of-plane hydraulic heads, may significantly enhance permeability in this direction.

These model results support the considerable body of evidence that fluid migration is broadly associated with regions of active faulting (Sibson 1989a). However, for fractured rock masses, the model indicates that enhanced fluid flow is not necessarily confined to the fault zone, but may extend into the hangingwall at shallow depths.

COMPARISON OF MODEL A WITH A SUPRA-HYDROSTATIC FLUID PRESSURE AT A GREATER DEPTH

Hydraulic boundary conditions at depth

The hydraulic boundary condition in Fig. 2 was used to simulate a fault region at shallow depth, where fractures were interconnected through to the surface. However, a transition towards supra-hydrostatic fluid pressure at depths of a few kilometres is reported in many sedimentary basins (Fertl *et al.* 1976, Sibson 1990). An alternative hydraulic boundary condition has been used to simulate the deformation and fluid flow at a depth of 2 km below the surface, based on the geometry of model A.

At such a depth, the total stress in the vertical direction, σ_1, was 50 and 51 MPa along the top and bottom boundaries, respectively. The total stress in the horizontal direction, σ_3, increased downwards along both the left and right boundaries from 24 to 24.48 MPa because of a lateral pressure ratio of 0.48. A hydrostatic fluid pressure of 0.4 was selected for the first 1500 m below the free surface and a supra-hydrostatic fluid pressure of 0.6 below 1500 m. Hence, the fluid pressure along the top boundary was 22.5 MPa and 23.1 MPa along the bottom boundary. The fluid pressure along both the left and right boundaries increased downwards from 22.5 to 23.1 MPa. Note that the effective stress was still compressive in all directions.

Comparison in characteristic behaviour

At greater depth, the fault region experiences a larger vertical stress and fluid pressure. During the period of fault slip, which was equivalent to 0.6 s real time, the hangingwall subsided by 1.1 m. Figure 8(a) shows the geometry after faulting.

Within the fault zone, a fairly uniform distribution of shear displacement existed. Many openings were created around the basement within the zone with rotation of blocks, as shown in detail in Fig. 8(b). There were rather different features of aperture distribution from the model at shallow depth. The apertures developed mainly within and around the lower part of the zone (Figs. 8c & d). From these distributions, it is evident that some fractures in local areas (including the fault zone, footwall and hangingwall) closed and others opened in response to local stress and fluid pressure changes around the blocks. The fractures in the lower part of the fault zone developed rather large apertures and would serve as the main channels for fluid flow (Figs. 8a & b). Again, such structures would increase the permeability greatly out of the plane studied here.

The porosity and average flow rates before and after faulting may be compared (Fig. 9). Increased porosity only developed within the fault zone, with slight decreases in the footwall and hangingwall. It is interesting to note that the average flow rate within the footwall and hangingwall decreased greatly and the flow rate within the zone only increased a little (Fig. 9b). This is due to stress concentrations reducing the apertures to the residual minimum value (a_{res} = 0.0005 m for sub-vertical fracture and 0.0001 m for sub-horizontal fractures). As a result, some obstructions formed locally in the pathways of fluid flow, and the average flow rate decreased.

EFFECTS OF IRREGULARITIES IN FAULT ZONE

Fault jogs are of interest because they have important effects on various geological processes. For example,

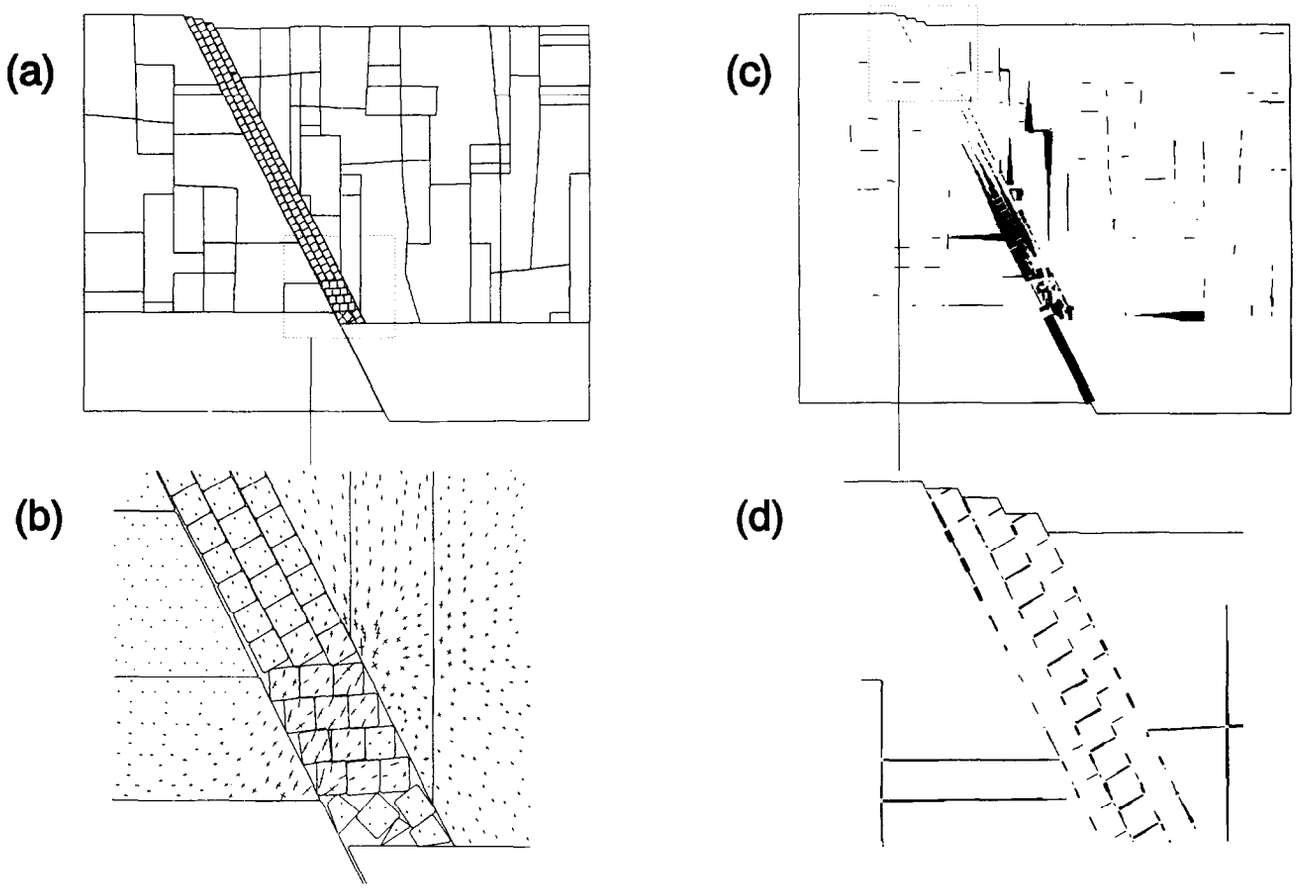

Fig. 8.(a) Geometry of model A, after fault slip, at a depth of 2000 m below the free surface. (b) Detail to show the stress redistribution and openings created around the base of the fault zone, with the formation of a channel along the basement/cover interface due to block movement. (c) Aperture distribution in this model, with greatest dilation near the base of the fault zone; each line represented an aperture of 0.0016 m. (d) Detail showing the aperture distribution around top of the fault zone; each line represented an aperture of 0.001 m.

jogs are important sites for earthquake initiation and termination, and for aftershock activity (King & Nabelek 1985). The structures which develop at jogs can make them important locations for hydrocarbon migration and entrapment (Larson 1988, Morley *et al.* 1990, Peacock & Sanderson 1994) and for mineralization (Dunham 1988). However, dilational jogs and anti-dilational jogs may play rather different roles in slip transfer along faults (Segall & Pollard 1980, Sibson 1987, Peacock & Sanderson 1991, 1992). In this study, the basic extensional fault model has been modified to include these features. Model B (Fig. 10a) shows the fault region with a dilational jog and model C (Fig. 11a) shows the fault region with an anti-dilational jog. The geometrical features and stress distributions from the UDEC models have been compared with structures developed around small-scale fault jogs (Peacock & Zhang 1994). The effect of dilational and anti-dilational jogs on deformation and fluid flow will be discussed in this section. The models differ from the basic geometry of model A only in the shape of the fault zone. The movement direction of basement in model B (Fig. 10a) and model C (Fig. 11a) is the same as that in Model A (Fig. 1) and the boundary conditions in Fig. 2 are applied so that the effects of irregularities on deformation and fluid flow can be compared.

Dilational fault jog

The geometry before fault slip is shown in Fig. 10(a); boundary conditions were applied as in Fig. 2. Fault slip occurred for a period of one second, producing 0.65 m subsidence of the hangingwall (Fig. 10b).

Relatively large openings developed in the fault zone and the hangingwall along fractures in two directions with marked rotation of blocks (Fig. 10b). The main difference from model A (straight fault zone) was that dilation developed rather more variably, particularly along the fault zone and within the hangingwall (Fig. 10c). Another distinct characteristic of the aperture distribution was that large dilations developed along some sub-horizontal fractures. This can be attributed to non-uniform subsidence at different levels in the hangingwall caused by the jog of the fault zone. As a result, large surface displacement occurred at some distance from the fault zone (Fig. 10b). These phenomena, including thickening, block rotation, void formation and stress decreases, are similar to those results

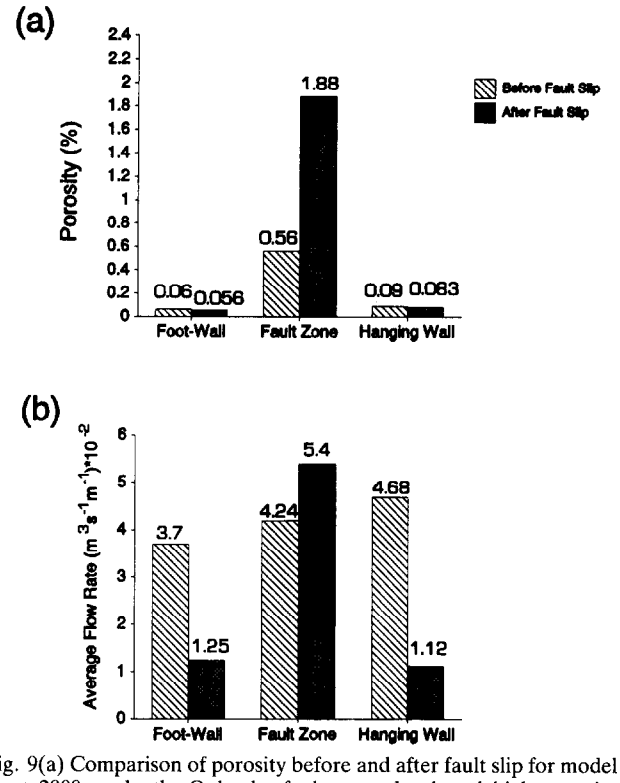

Fig. 9(a) Comparison of porosity before and after fault slip for model A at 2000 m depth. Only the fault zone developed high porosity (increasing from 0.56 to 1.88%), with the footwall and hangingwall showing little change. (b) Comparison of average flow rates before and after fault slip. The average flow rate within the footwall and hangingwall are reduced and that within the fault zone only increases slightly.

obtained from earlier models of dilational fault jogs (Peacock & Zhang 1994).

Anti-dilational (or contractional) fault jog

For model C (Fig. 11a) with boundary conditions as in Fig. 2, fault slip occurred for a period of one second, producing 0.5 m subsidence of the hangingwall. The geometry after fault slip is shown in Fig. 11(b).

The aperture distribution of this model after fault slip is shown in Fig. 11(c), from which it is evident that the main dilation occurred within the fault zone and hangingwall. In the restraining jog itself, dilation was reduced due to the high compressive stress. This is compatible with the thinning of beds and radial fractures at contractional jogs on faults at Flamborough Head, England (Peacock & Zhang 1994). On the other hand, large dilations developed in the steeper, dilational section along adjacent sub-horizontal fractures, which resulted from the non-uniform slip at different heights in the hangingwall block. The main difference from model B is that fractures developed more variable apertures within the fault zone and generally lower values within the hangingwall.

DISCUSSION OF DYNAMIC RESPONSE OF FLUID-DILATION INTERACTIONS

Dynamic behaviour has received relatively little attention in the literature. For example, Sibson (1989a)

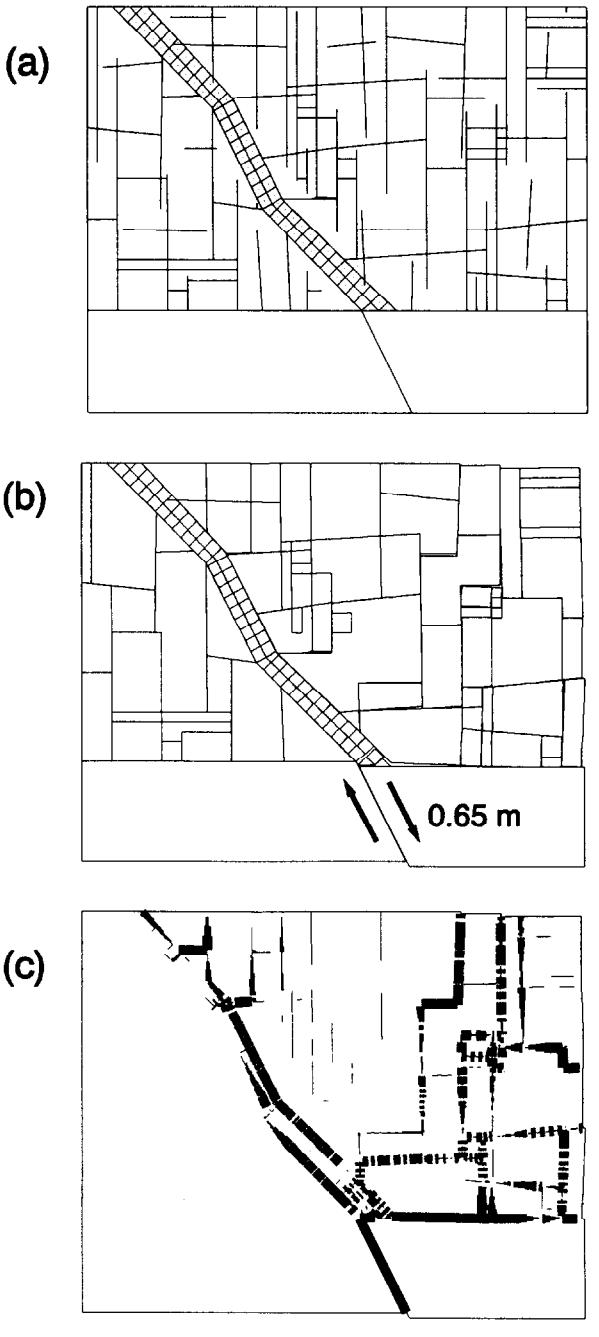

Fig. 10.(a) Geometry of model B before fault slip; the fault region consists of a fault zone with a dilational jog and regional joints. (b) Geometry after fault slip at a shallow depth (the boundary conditions in Fig. 2 were applied). Some openings were created within the fault zone and the hangingwall due to initial loading. Surface displacement occurred away from the fault zone. (c) Aperture distribution for this model after fault slip; the main dilation is within the fault zone and hanging wall.

noted that ". . . most structural geologists and mining geologists have traditionally viewed fault zones in a somewhat static manner, paying much attention to the stress fields responsible for their initiation and viewing their evolution in terms of smooth progressive deformation . . .". Some reasons which inhibit such investigations may be attributed to the difficulty of obtaining evidence of dynamic processes in ancient tectonic structures and in carrying out physical simulation of such processes. However, numerical modelling can provide a powerful approach to such dynamic simulation as long as

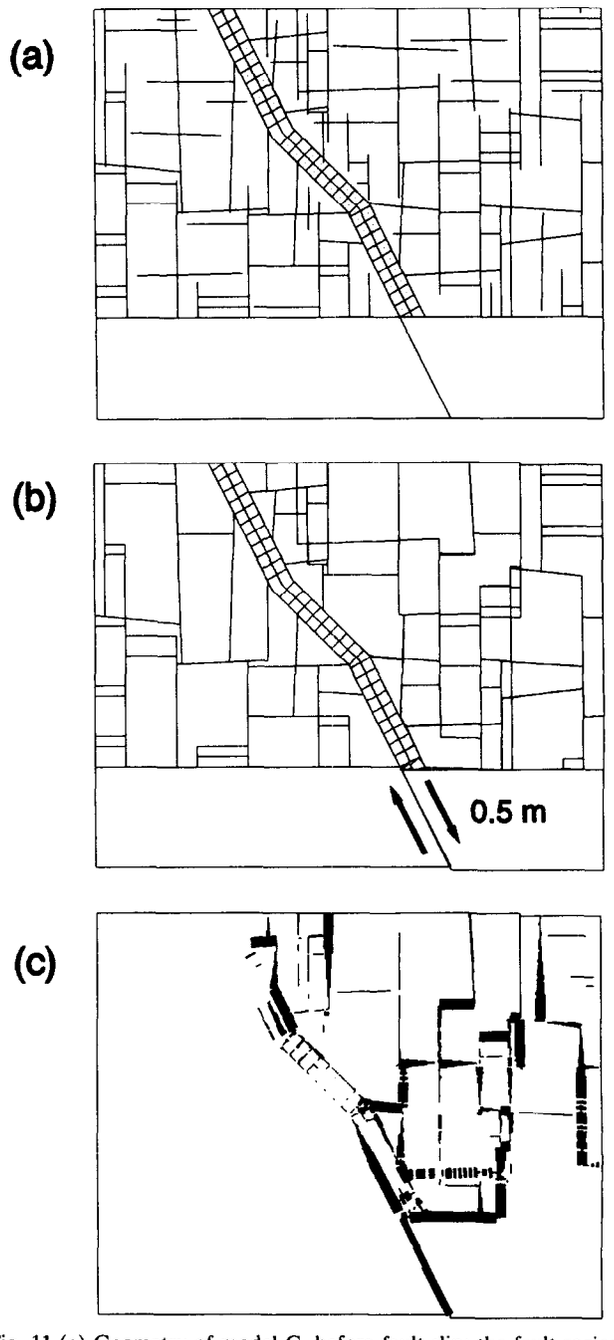

Fig. 11.(a) Geometry of model C, before fault slip; the fault region consists of a fault zone with an anti-dilational jog and regional joints. (b) Geometry after fault slip at a shallow depth. (c) The aperture distribution shows closing of fractures in the fault zone at the anti-dilational jog and the opening of fractures in the hangingwall adjacent to the steeper, dilational sections of the fault zone.

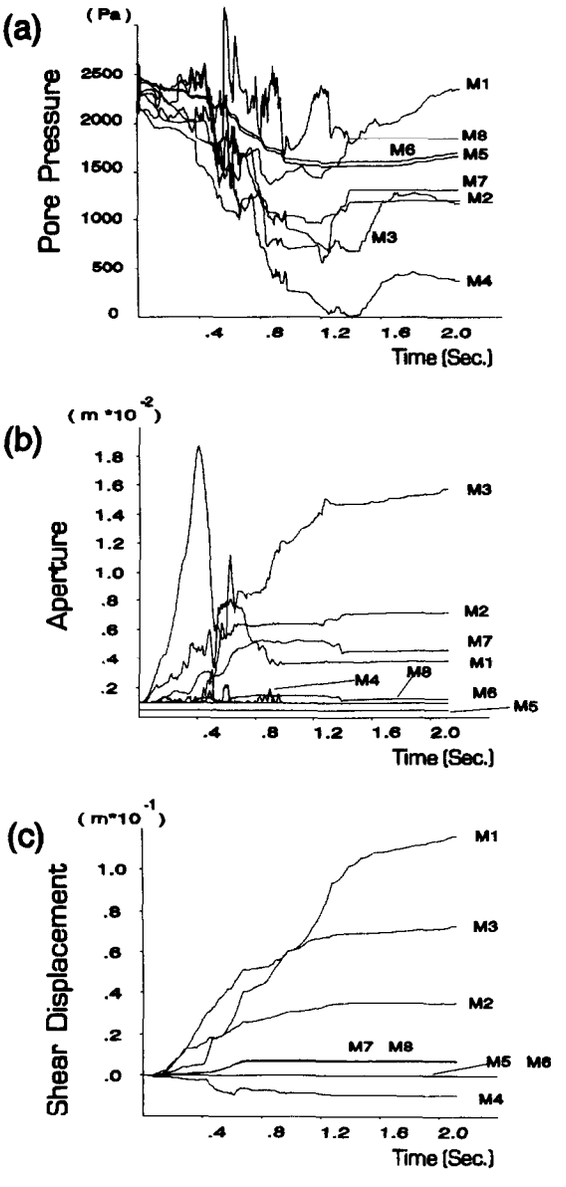

Fig. 12. Variations in (a) pore pressure, (b) aperture and (c) shear displacement with time in Model A. Symbols M1–8 refer to various monitored sites, see Fig. 1.

it is based on correct constitutive relationships and reasonable boundary conditions.

That fluids are intimately involved in the faulting process is clear from examples of earthquakes triggered by pore pressure increases (for example, Talwani & Acree 1985) and observations of post-seismic fluid discharge (Briggs & Troxell 1955, Sibson 1981). Dynamic faulting, associated with fluid flow, is also important to the understanding of hydrothermal mineral deposition (Newhouse 1942, Sibson 1990).

During a period of tectonic activity, fluid flow through a faulted region is controlled by fluid pressure variation and the dilation or closure (anti-dilation) of fractures. Thus, fluid flow, deformation and slip on active faults are controlled not only by the geological and tectonic setting, but also by the coupled mechanical and hydraulic behaviour of the rock mass. The UDEC models, although designed mainly to compare stress and fluid flow before and after fault slip, can be used to gain some insight into the dynamic response during the period of fault slip.

Figure 12 shows the dilation, fluid pressure and shear displacement at eight monitored fractures during the period of the simulation in model A at a shallow depth. There were generally two main phases of fluid pressure fluctuation at each monitored fracture. During the fault slip, fluid pressure dropped (Fig. 12a) and then tended to rise gently until the end of the simulation. The fluid pressure did not completely recover after faulting, due to the short duration of monitoring.

In the fault zone (M1, M2, M3 and M4) and hangingwall (M7 and M8), pressure fluctuations were most pronounced, and can be attributed to local block movements. The pressure variation in the footwall (M5 and M6) was much smoother. It is interesting to note that the variations of fluid pressure at different positions monitored in the same local area were very similar to each other.

During the fault slip, there were rapid fluctuations in the apertures of the fractures (Fig. 12b), particularly in the fault zone and hangingwall. Both the aperture and shear displacement (Fig. 12c) reached a steady state at the end of the 2 s monitoring period, i.e. within a time span equivalent to the period of slip. The greatest finite change in aperture and shear displacement occurred on the steep fractures within the fault zone (M1, M2 and M3), which also showed the most fluctuation during the period of slip.

In the early stage of faulting (0–0.6 s), the slip was accompanied by rapid dilation, but with only limited shear displacement. The dilation of fractures was transferred by limited slip within the fault zone. At a later stage (0.6–1.2 s), steep fractures within the fault zone developed high shear displacement with varying rates. Comparison of the shear displacement history of M1, M2 and M3 suggests a longer duration of the slip event (rupture time) as one passes up the fault plane. Towards the end of the monitoring period, there was little change taking place in aperture and shear displacement, although fractures in the hangingwall and fault zone display a finite opening. Recovery of fluid pressure was not achieved over the period of monitoring.

Similar features were seen in the other models, with a concentration of dilation and shear displacement within the fault zone being more apparent at greater depth. More extensive monitoring within the models and the use of longer periods of slip might provide more detailed information, especially on the variation of fluid flow around jogs in the fault zone and on the linkage of the flow in the hangingwall and fault zone. The changes are also of great significance for the development of hydrothermal veins, where dilation created during fault slip and the transient pressure drops might allow influx of fluids into the fault zone. The progressive increase in duration of the shear displacement and dilation up the fault zone might also facilitate rapid fluid transport along the zone.

Textures characteristic of incremental vein growth are increasingly recognized in fault-related mineralization (Cox & Etheridge 1983, Cox 1987, Sibson 1989b). The development of arrays of sub-vertical hydrothermal extensional veins in the vicinity of normal faults might be a major factor contributing to the association of epithermal mineralization within extensional fault systems.

CONCLUSIONS

The UDEC has been used to model fluid flow and deformation in extensional fault regions. The results observed from these models suggest that fault slip has significant effects on distribution of dilation ('porosity'), fluid pressure fluctuation, stress redistribution and fluid flow. The dynamic fluid-fault interactions during a single faulting episode are complex. Although aimed at an understanding of mineralization in extensional fault regions, the methodology and results presented here have wide implications in other fields. Some points can be drawn from these models:

(1) After fault slip, local dilation of fractures occurs within the fault zone. This result is largely independent of the geometry of the fault zone and produces marked increases in the 'porosity' and permeability of the fault zone, particularly in the third dimension because extensional structures likely form a highly permeable channel out of the vertical section studied here; the latter may increase by several orders of magnitude in the models studied.

(2) At shallow depths, dilation of fractures and associated fluid flow extends into the hangingwall, although this effect is much less pronounced at depth.

(3) Jogs in the fault zone cause major variations in the distribution of stress and dilation. Anti-dilational jogs may be sites for reduced dilation and flow within the fault zone, but local stress concentrations and block movements can generate dilation in the hangingwall, even at greater depth.

(4) Fault slip can cause transient fluctuations in dilation and fluid pressure locally, with pressure drops of 0.2 MPa at shallow depth and 2.7 MPa at 2 km depth. These induced pressure differentials may be important in drawing fluid into a fault zone and may explain the suction-pump mechanism of Sibson (1989a).

(5) Where the fluid flow is accompanied by migration and precipitation of ores, the models predict that high level mineralization (epithermal, Mississippi Valley type, etc.) will be preferentially developed in the hangingwall and fault zone, where dilation is greatest.

Acknowledgements—This work was supported by a research grant (GR9/915) from the Natural Environment Research Council, U.K. The authors would like to thank Richard Harkness, Nigel Last and David Peacock for advice at various stages of this project and Rick Sibson, Dick Norris and an anonymous reviewer for constructive reviews.

REFERENCES

Barton, N. R., Bandis, S. & Bakhtar, K. 1985. Strength, deformation and conductivity coupling of rock joints. *Int. J. Rock Mech. & Mining Sci. Geomech. Abstr.* **22**, 121–140.

Barton, C. C. & Hsieh, P. A. 1989. Physical and hydraulic-flow properties of fractures. *28th Int. Geol. Congr.* Field Trip Guidebook **T-385**, 1–31.

Briggs, R. C. & Troxell, H. C. 1955. Effect of Arvin-Tehachap earthquake on spring and streamflow. *Cal. Div. Mines & Geol. Bull.* **171**, 81–98.

Cox, S. F. 1987. Antitaxial crack-seal vein microstructures and their relationship to displacement paths. *J. Struct. Geol.* **9**, 779–789.

Cox. S. F. & Etheridge, M. A. 1983. Crack-seal fibre growth mechanisms and their significance in the development of oriented layer silicate microstructure. *Tectonophysics* **92**, 147–170.

Cundall, P. A., Marti, J., Beresford, P., Last, N. C. & Asgian, M. 1978. Computer monitoring of jointed rock masses. *U.S. Army Eng. WEST Tech. Rep.* N-78-4.

Das, S. & Scholz, C. H. 1981. Theory of time-dependent rupture of the earth. *J. geophys. Res.* **86**, 6039–6051.

Dunham, K. C. 1988. Pennine mineralisation in depth. *Proc. Yorks. Geol. Soc.* **47**, 1–12.

Fertl, W. H., Chilingarian, G. V. & Rieke, H. H. 1976. *Abnormal Formation Pressures.* Elsevier, Amsterdam.

Healy, J. H., Rubey, W. W., Griggs, D. T. & Raleigh, C. B. 1968. The Denver earthquakes. *Science* **161**, 1301–1310.

Heffer, K. J. & Bevan, T. G. 1990. Scaling relationships in natural fractures: data, theory and application. *SPE 20981*, 367–376.

Jaeger, J. G. & Cook, N. G. W. 1979. *Fundamentals of Rock Mechanics*, 3rd edn. Chapman & Hall, London.

King, G. C. P. & Nabelek, J. 1985. Role of fault bends in the initiation and termination of earthquake ruptures. *Science* **288**, 984–987.

Knipe, R. J. 1993. Faulting processes, fluid flow and the evolution of reservoir compartments. In: *Geofluids '93 Ext. Abstr.* (edited by Parnell, J. *et al.*). 134–136.

Larson, P.-H. 1988. Relay structures in a lower Permian basement-involved extensional system, east Greenland. *J. Struct. Geol.* **10**, 3–8.

Last, N. C. & Harper, T. R. 1990. Response of fractured rock subject to fluid injection Part 1. Development of a numerical model. *Tectonophysics* **172**, 1–31.

Lorenz, J. C. & Finley, S. J. 1991. Regional fractures II: fracturing of mesaverde reservoirs in the Piceance Basin, Colorado. *Bull. Am. Ass. Petrol. Geol.* **75**, 1738–1757.

Lorenz, J. C., Teufel, L. W. & Warpinski, N. R. 1991. Regional fractures I: a mechanism for the formation of regional fractures at depth in flat-lying reservoirs. *Bull. Am. Ass. Petrol. Geol.* **75**, 1714–1737.

Louis, C. 1969. A study of groundwater flow in jointed rock and its influence on the stability of rock mass. *Imperial College Rock Mech. Rep.* **10**.

Morley, C. K., Nelson, R. A., Patton, T. L. and Munn, S. G. 1990. Transfer zone in the East African rift system and their relevance to hydrocarbon exploration in rifts. *Bull. Am. Ass. Petrol. Geol.* **74**, 1234–1253.

Newhouse, W. H. 1942. *Ore Deposits as Related to Structural Features.* Princeton University Press, Princeton, New Jersey.

Peacock, D. C. P. & Sanderson, D. J. 1991. Displacement, segment linkage and relay ramps in normal fault zones. *J. Struct. Geol.* **13**, 721–733.

Peacock, D. C. P. & Sanderson, D. J. 1992. Effects of layering and anisotropy on fault geometry. *J. geol. Soc. Lond.* **149**, 793–802.

Peacock, D. C. P. & Sanderson, D. J. 1994. Geometry and development of relay ramps in normal fault systems. *Bull. Am. Ass. Petrol. Geol.* **78**, 147–165.

Peacock, D. C. P. & Zhang, X. 1994. Field examples and numerical modelling of oversteps and bends along normal faults in cross-section. *Tectonophysics* **234**, 147–167.

Pine, R. J. & Cundall, P. A. 1985. Applications of the fluid–rock interaction program (FRIP) to the modelling of hot dry rock Geothermal Energy Systems. *Proc. Int. Symp. on Fundamentals of Rock Joints*, Bjorkliden, 293–302.

Raleigh, C. B., Healy, J. H. & Bredehoeft, J. D. 1976. An experiment in earthquake control at Rangely, Colorado. *Science*, **191**, 1230–1237.

Rosso, R. S. 1976. A comparison of joint stiffness measurements in direct shear, triaxial compression and *in situ*. *Int. J. Rock Mech. & Mining Sci. Geomech. Abstr.* **13**, 167–172.

Segall, P. & Pollard, D. D. 1980. Mechanics of discontinuous faults. *J. geophys. Res.* **85**, 4337–4350.

Segall, S. W. & Pollard, D. D. 1983. Joint formation in granitic rock of Sierra Nevada. *Bull. geol. Soc. Am.* **94**, 563–575.

Sibson, R. H. 1981. Fluid flow accompanying faulting: field evidence and models. In: *Earthquake Prediction: an International Review. Am. geophys. Un. Monogr., Maurice Ewing Ser.* **4**, 593–603.

Sibson, R. H. 1987. Earthquake rupturing as a hydrothermal mineralizing agent. *Geology* **15**, 701–704.

Sibson, R. H. 1989a. Earthquake faulting as a structural process. *J. Struct. Geol.* **11**, 1–14.

Sibson, R. H. 1989b. Structure and mechanics of fault zones in relation to fault-hosted mineralization. *Aust. Miner. Found.* Adelaide.

Sibson, R. H. 1990. Faulting and fluid flow. In: *Short Course on Fluids in Tectonically Active Regions of the Continental Crust* (edited by Nesbitt, B. E.). Mineralogical Association of Canada Handbook **18**, 93–132.

Snow, D. T. 1968. Rock fracture spacings, openings and porosities. *J. Soil. Mech. Found. Div. ASCE* **94**(SMI), 73–91.

Talwani, P. & Acree, S. 1985. Pore pressure diffusion and the mechanism of reservoir-induced seismicity. *Pure & Appl. Geophys.* **122**, 947–965.

Yerkes, R. E., Levine, P. & Wentworth, C. M. 1985. Abnormally high fluid pressure in the region of the Coalinga earthquake—a preliminary report. *U.S. Geol. Surv.* Open-File Report **85-44**, 344–375.

Witherspoon, P. A., Wang, J. S. Y., Iwai, K. & Gale, J. E. 1980. Validity of cubic law for fluid flow in deformable rock fracture. *Water Resour. Res.* **16**, 1016–1024.

Yoshnaka, R. & Yamabe, T. 1986. Joint stiffness and the deformation behaviour of discontinuous rock. *Int. J. Rock Mech. & Mining Sci. Geomech. Abstr.* **23**, 19–28.